Jordanian Journal of Computers and Information Technology (JJCIT), Vol. 12, No. 01, March 2026.

AMBIENT BACKSCATTER-ASSISTED PASSIVE RELAYING WITH ENERGY HARVESTING: PERFORMANCE ANALYSIS

Lam-Dong Huynh[1], Lam-Thanh Tu[2], Quang-Sang Nguyen[3] and Tan N. Nguyen[2]

(Received: 11-Dec.-2025, Revised: 1-Feb.-2026, Accepted: 22-Feb.-2026)

ABSTRACT

Ultra-energy-efficient communication solutions are required as Internet of Things (IoT) devices proliferate in the shift to 6G networks. In this paper, a novel architecture that uses energy harvesting (EH) protocols to integrate Ambient Backscatter Communication (AmBC) as a passive relay is investigated. An energy-constrained backscatter device uses a power splitting (PS) mechanism to both reflect its information to the destination and harvest energy for circuit activation. The main contribution of this work is the development of new and accurate closed-form expressions for the system outage probability (OP) over Rayleigh fading channels. Extensive Monte Carlo simulations are conducted to rigorously validate the accuracy of the proposed analytical framework. The analysis reveals important trade-offs between transmission reliability and energy-harvesting efficiency, providing valuable insights for resource optimization in future low-power IoT networks. The results demonstrate that the adverse effects of imperfect successive interference cancellation (SIC) and/or imperfect channel state information (CSI) can be effectively mitigated by increasing the transmit power and/or operating at the optimal value of the reflection coefficient. Moreover, the performance gap between perfect and imperfect SIC and CSI is shown to be relatively small. Finally, we analytically prove that the linear EH model serves as an upper bound for the practical nonlinear EH model.

KEYWORDS

Ambient backscatter communication, Energy harvesting, Outage probability, Relay-assisted network, Imperfect successive interference cancellation, Imperfect channel state information.

1. INTRODUCTION

The proliferation of IoT devices during the transition phase from 5 G to 6 G is driving an escalating demand for ultra-energy-efficient, low-cost communication solutions capable of supporting wide-area connectivity for billions of low-power sensor devices. Recent surveys on the 6 G vision emphasize that future networks must achieve an unprecedented level of dense connectivity, high energy efficiency, and support for near-zero-power IoT nodes [1]-[2]. Furthermore, 6G is being defined as an "Intelligent Network of Everything," where ultra-light, ultra-energy-efficient devices play a critical role in maintaining continuous sensing and communication capabilities [3]. These stringent requirements have spurred intense interest in low-power communication technologies, with AmBC and Wireless Energy Harvesting (WEH) emerging as highly promising solutions due to their ability to reuse ambient signals for communication without requiring an active power source.

To address these connectivity challenges, AmBC has emerged as a particularly critical paradigm, enabling passive devices to communicate by harvesting and reflecting existing radio frequency (RF) signals present in the environment. By not requiring an active RF transmitter, AmBC offers significant advantages in terms of power consumption, cost, and sustainability, making it naturally suited for the development of ultra-energy-efficient IoT systems in the near future [4]. Numerous surveys have comprehensively summarized the principles, system models, challenges, and application directions of AmBC in the field of wireless communication [4]. Beyond the fundamental architectures, extensive research has explored the integration of AmBC with key 6G technologies, such as artificial intelligence (AI), non-terrestrial networks (NTNs), or intelligent platforms, to expand the application space and enhance system performance [5]-[6]. In the context of NTNs, recent studies have further analyzed the

1. L.-D. Huynh is with the Faculty of Electrical and Electronics Engineering, Ton Duc Thang University, Ho Chi Minh City, Vietnam. Email: huynhlamdong.st@tdtu.edu.vn
2. L.-T. Tu and Tan N. Nguyen (Corresponding Author) are with the Advanced Intelligent Technology Research Group, Faculty of Electrical and Electronics Engineering, Ton Duc Thang University, Ho Chi Minh City, Vietnam. Emails: tulamthanh@tdtu.edu.vn and nguyennhattan@tdtu.edu.vn
3. Q.-S. Nguyen is with the Posts and Telecommunications Institute of Technology, Ho Chi Minh City, Vietnam. Email: sangnq@ptit.edu.vn

secure performance of satellite-terrestrial networks assisted by backscatter devices to ensure reliability in wide-area IoT deployments [7]. More specialized research directions have also been developed to address the specific challenges of AmBC. For instance, solutions for enhancing coverage and link quality by integrating smart surfaces, like Reconfigurable Intelligent Surfaces (RISs)/Intelligent Reflecting Surfaces (IRSs), have been proposed in several recent works [6][8][9][10]. Meanwhile, studies related to security and privacy focus on analyzing secrecy performance, covert operations, or UAV-assisted AmBC scenarios, thereby assessing the reliability of backscatter systems in complex environments [11][12][13]. In addition, many studies have concentrated on signal detection and decoding techniques, especially in the context where backscatter signals are weak and susceptible to interference from active sources or environmental noise. Methods, such as machine learning-based detection and blind detection, have been developed to improve signal reception efficiency [14]-[15]. Some research also targets hybrid or more advanced architectures, such as LTE-uplink-based AmBC [16], hybrid relay-backscatter systems with energy harvesting [17], NOMA-assisted AmBC, advanced symbiotic radio networks aided by STAR-RIS to maximize IoT throughput [18], or advanced short-packet IoT systems that improve Block Error Rate (BLER) in RIS environments [19] and cooperative/mutualistic AmBC models considering the effects of hardware impairments [20]. Moreover, joint time and energy-management strategies using deep reinforcement learning have been explored in backscatter-assisted hybrid underlay cognitive radio networks (CRNs) to enhance resource efficiency [21]. Furthermore, the performance of device-to-device (D2D) Partial NOMA-assisted Backscatter Communication architectures has been analyzed to evaluate the benefits of combining NOMA and D2D in backscatter systems, particularly in high-density IoT scenarios [22]. Additionally, the impact of co-channel interference on energy harvesting within D2D networks has been investigated, specifically focusing on symbol error-rate analysis under power beacon-assisted configurations [23]. Furthermore, recent advancements in D2D-enabled cellular networks have explored joint throughput maximization and Age of Information (AoI) constraints using deep reinforcement learning to optimize energy-harvesting efficiency [24]. Overall, the current research directions have formed a rich landscape for AmBC, spanning from foundational principles [4], integration with AI and 6 G platforms [5], to the vision of performance enhancement using RISs/IRSs [6], [8]-[10], security solutions [11]-[13], and practical detection-decoding designs and deployment models [10], [13]-[17], [19]-[20].

While AmBC provides an efficient reflection mechanism, the autonomous operation of these devices is fundamentally dependent on a sustainable power supply. Consequently, EH techniques have emerged as a key solution, allowing devices to scavenge energy from the ambient environment (e.g., RF electromagnetic fields, light, heat, or vibration) and convert it into useful electrical power to supply electronic circuits or small storage units. Due to its ability to provide a continuous power source at very low power levels, EH has remained a leading research area in recent years and is gaining increasing attention in subsequent network generations, particularly for ultra-low-power IoT systems [25]-[26]. Specifically, at the hardware and antenna structure level, much research focuses on optimizing the design of antennas, metantennas, and meta-materials to enhance energy-conversion efficiency in the ISM band or other target frequency ranges, thereby increasing the harvested power and improving the efficiency of practical EH systems. Advances in meta-materials/meta-surfaces and metantennas demonstrate the potential for boosting energy capture and increasing deployment flexibility in industrial or civilian scenarios [27]-[29].

Building upon these hardware advancements, at the network layer, EH has been widely integrated into various system designs to support node autonomy: from NOMA-based IoT networks with EH to cooperative relay/DF systems with self-energy recycling mechanisms or UAV-assisted relaying scenarios, where EH plays a pivotal role in balancing reliability and information security. This security-reliability trade-off is also explored through the use of multi-antenna diversity combined with energy harvesting to safeguard wireless communications against eavesdropping [30]. Studies also investigate the trade-off between reliability and security when utilizing EH in relay-assisted UAV communications [31]-[34]. Complementary to these studies, the co-design of clustering, transmission, and trajectory for UAV-assisted Wireless Powered Communication Networks (WPCNs) has been proposed to minimize AoI, ensuring fresh data delivery in energy-constrained environments [35]. Another direction is the combination of EH with intelligent environmental platforms, like RISs-both in the context of energy harvesting for autonomous RISs and in network designs supporting federated learning (FL), where the optimization of RF-EH resource allocation impacts the FL performance. Works on autonomous RISs and EH network optimization for advanced tasks (e.g., federated learning) reflect the trend of tightly

integrating communication, distributed processing, and energy management [36]-[37]. Finally, EH is also being considered in practical applications and specific scenarios-from intelligent military logistics based on IoT and EH to physical layer-security solutions utilizing friendly jammers to assist energy-harvesting sensor networks. These results indicate that EH is not merely a hardware-design topic, but also a foundational research axis closely linked to challenges in security, resource allocation optimization and multi-context applications within the 5G/6G ecosystem [38]-[39].

1.1 Motivation and Contribution

The synergy between AmBC and EH represents an ideal strategy for developing ultra-energy-efficient IoT networks. The primary objective of merging these two techniques is to leverage ambient energy to power backscatter devices and utilize supporting relay nodes to extend connectivity range, thereby addressing the needs of massive IoT scenarios. In recent years, the integration of AmBC and EH has garnered significant research interest, leading to a diverse range of studies focusing on different network architectures and optimization goals. Comparative performance studies between backscatter communication and energy harvesting in large-scale IoT networks have elucidated the respective advantages and limitations of each solution, laying the groundwork for hybrid models [40]. Analyses based on Stochastic Geometry (SG) have evaluated the performance of backscatter networks powered by ambient RF energy, providing key metrics, such as outage probability and throughput, in random environments [41]. Complementing these theoretical frameworks, a comprehensive survey has systematically reviewed the practical applications and potential deployment of AmBC in battery-free IoT, emphasizing the necessity of integrating EH to sustain continuous operation [42]. As the field has matured, researchers have begun exploring specialized platforms to further enhance system capability. Specific studies have investigated the use of RISs to simultaneously support backscattering and energy harvesting, thereby improving coverage and enhancing throughput and reliability performance [43]. Additionally, minimizing the Age of Information (AoI) in ambient backscatter-assisted EH-CRNs through cooperative spectrum sensing has emerged as a key approach to maintain data freshness in IoT applications [44]. Meanwhile, hybrid models in cognitive radio networks have been proposed to maximize throughput for backscatter-aided EH networks, demonstrating the feasibility of flexible channel-management mechanisms [45]. In a similar vein, within heterogeneous CRN environments, optimal time-allocation policies have been developed for backscatter-aided relay cooperative transmission to balance harvesting and transmission needs [46]. Further investigations have focused on optimizing transmission protocols and hardware configurations. Opportunistic backscatter protocols have also been developed to optimize energy usage and boost data-transmission performance in EH-assisted IoT networks [47]. Research on relay-assisted cooperative transmission has shown that optimal relay selection in EH-backscatter networks significantly improves throughput and reduces latency, while ensuring continuous operation for battery-free devices [48]. Moreover, the throughput maximization of WPCNs has been further enhanced by employing mobile access points to mitigate the doubly near-far problem and improve energy-transfer efficiency [49]. Optimal control policies for RF-powered backscatter networks have been proposed to balance harvested energy and data-transmission capability [50]. Finally, to address more complex operational requirements, outage analyses in EH-assisted relay networks with backscatter have provided crucial closed-form expressions for system performance evaluation [51]. To accommodate the demands for hybrid long- and short-packet data transmission, numerous works have explored HARQ mechanisms, hybrid packet scheduling, and cooperative relaying for AmBC with EH, aiming to enhance reliability and throughput [52]-[54]. Finally, the combination of EH with cooperative NOMA in two-user backscatter networks has demonstrated the potential to improve communication performance, optimize energy utilization, and address complex IoT scenarios [55].

Despite the recent concentration of research on integrating AmBC with EH [40]-[43], [45], [47]-[48], [50]-[55], a critical gap remains in the literature. Most of these works often focus on throughput or hybrid packet-performance scenarios without a comprehensive analysis of the OP in relay-assisted networks under realistic hardware and channel impairments. For example, studies on opportunistic backscatter [47] or relay selection-based cooperative backscatter [48] primarily aim to maximize throughput without providing closed-form expressions for OP. The hybrid long-short packet models [50]-[52] improve reliability for mixed-packet scenarios, but do not optimally exploit the capabilities of energy harvesting combined with backscatter in a relay environment. Even works concerning cognitive

radio networks [45] or D2D Partial NOMA-assisted backscatter [22] do not thoroughly consider the practical constraints of interference cancellation and channel estimation in the outage performance evaluation. In summary, previous methodologies have not simultaneously addressed three key factors: (i) using backscatter for energy efficiency, (ii) exploiting ambient-energy harvesting PS protocol, (iii) analyzing OP performance in a relay-assisted scenario, the impact of imperfect SIC, and the consequences of imperfect CSI due to estimation errors, which are crucial for assessing the practical reliability of IoT networks. To fill this void, our work focuses on ambient backscatter-assisted relaying, with the objective of calculating accurate closed-form expressions for the OP. Compared to previous studies, our work simultaneously combines AmBC and relay-assisted transmission while specifically focusing on OP, constituting a novel, important, and urgent contribution for the deployment of ultra-energy-efficient IoT networks in the 5G/6G era. The main contributions of this paper are summarized as follows:

- We propose a hybrid symbiotic radio framework in which an ambient backscatter device acts as an energy-harvesting-assisted passive relay. Unlike conventional SWIPT systems, the backscatter device is a passive (or semi-passive) node without an active RF transmitter and does not decode the source signal. Instead, it modulates its information by adjusting the reflection coefficient of the incident RF signal. The harvested energy is used solely for circuit activation, while a power-splitting scheme controls the trade-off between harvested energy and reflected signal strength rather than information decoding and energy harvesting.
- We provide a rigorous theoretical analysis of the system performance over Rayleigh fading channels. Specifically, we derive novel closed-form expressions for the OP, taking into account both ideal and imperfect Successive Interference Cancellation (imSIC) mechanisms at the receiver. These expressions, validated by extensive Monte-Carlo simulations, serve as a precise mathematical tool to evaluate the reliability and quantify the symbiotic benefits of the proposed system under residual interference and various channel conditions.
- Our analytical framework's accuracy is rigorously validated through comprehensive Monte-Carlo simulations. The numerical results clearly demonstrate how key parameters - including transmit SNR, target data rates, and channel conditions - directly influence system performance. This thorough investigation provides compelling evidence that our approach reliably captures the essential dynamics affecting overall efficiency and effectiveness.

Table 1. Comparison of the uniqueness of our research to related articles.

Context	EH protocol	EH Modeling	Relay-assisted	AmBC	OP
Paper [7]	TS	Linear	✓	✓	✓
Paper [21]	TS	Linear		✓	✓
Paper [23]	TS	Linear	✓		✓
Paper [31]	PS	Linear	✓		✓
Paper [32]	TS	Linear	✓		✓
Paper [40]	TS	Linear		✓	
Paper [41]	Hybrid TS - PS	Non - linear		✓	✓
Paper [42]				✓	
Paper [45]	Hybrid Action Selection	Linear		✓	
Paper [46]	TS	Linear	✓	✓	
Paper [47]	TS	Linear		✓	
Paper [48]	TS	Linear	✓	✓	
Paper [50]	TS	Linear		✓	
Paper [52]		Non - linear		✓	✓
Paper [55]	TS	Linear	✓	✓	✓
This paper	PS	Linear and Non-linear	✓	✓	✓

The remainder of the paper is organized as follows. Section 2 gives an overview of the system model. Section 3 presents the information-theoretic mathematical framework, to achieve the performance of the system. Section 4 presents numerical results and discussion to validate the developed framework as well as deeply explore the impacts of system key parameters, while Section 5 provides concluding remarks.

Jordanian Journal of Computers and Information Technology (JJCIT), Vol. 12, No. 01, March 2026.

2. SYSTEM MODEL

Figure 1 illustrates the proposed hybrid wireless communication system model, which has been widely investigated, set within a dense urban environment. The system comprises three main entities: a high-power Source (S), an energy-constrained Backscatter device (B), and an end Device (D)[1]. S serves as the primary access point, simultaneously transmitting the RF signal for energy provisioning and the data signal. B operates by harvesting RF energy from S *via* the Energy-harvesting link (green line). Concurrently, B modulates its own information onto the incident RF signal and reflects it towards D, forming one component of the Information links (black lines). The ultimate receiver, D, collects information through a combination of the conventional direct link from S and the backscatter link from B. This model is designed to thoroughly investigate the trade-off and co-existence between energy efficiency (enabled by B) and overall communication performance in the system. The mechanism for signal distribution and energy provision is realized through the PS scheme at S, with a total transmit power P_S over a transmission-block duration T. The system utilizes a reflection coefficient $\beta (0 \leq \beta \leq 1)$ to divide P_S into two streams supporting the backscatter link: a fraction $(1-\beta)P_S$ is allocated for the energy-harvesting process at B to power the device, while the remaining fraction βP_S is used to generate the RF backscattering signal, which acts as the carrier wave for B's data modulation. This modulated signal is then reflected by B towards D. Concurrently, the conventional direct communication link from S to D is maintained with a constant power P_S. D collects information through a combination of the direct link and the backscatter link. This PS scheme is crucial, as it enables the system to control the critical trade-off between the harvested energy at B and the received power of the backscattered signal at D, thereby optimizing the overall system performance and energy efficiency.

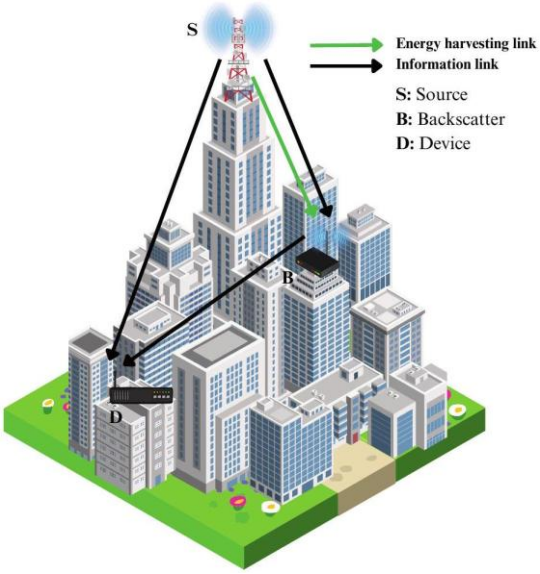

Figure 1. System model.

Let us denote h_{SD}, h_{SB}, h_{BD} as channel coefficients of the direct link from source node S to destination node D, and S → B, B → D links, respectively. We assume Rayleigh fading channels. Channel gains $h_X, X \in \{SB, BD, SD\}$ are exponential random variables (RVs) the probability density function (PDF) and cumulative distribution function (CDF) of which are given as, respectively.

$$f_{\gamma_X}(x) = \lambda_X \exp(-\lambda_X x)$$
$$F_{\gamma_X}(x) = 1 - \exp(-\lambda_X x) \quad (1)$$

where λ_X is mean of RV X. To take into account the simple path-loss model, we can formulate the parameters as follows:

$$\lambda_X = (d_X)^{\omega}, \quad (2)$$

[1] Although the considered AmBC system involves a single backscatter device equipped with a single antenna, our work explicitly incorporates energy harvesting with an energy-sufficiency constraint and derives closed-form expressions to characterize whether the harvested energy is sufficient for backscatter operation and signal decoding, thereby providing insights not captured in existing studies.

where ω is the path-loss exponent and d_X is the distance between two respective nodes. In a practical linear energy-harvesting paradigm, the average received power P_h at the BD is expressed as:

$$P_h = (1-\beta)P_S\gamma_{SB}. \tag{3}$$

If $P_h < P_{th}$, then B (Backscatter device) does not have enough energy to backscatter the signal from S to D. Thus, the received signal at D is written as: where P_{th} is the saturation threshold of the rechargeable power of the hardware circuit.

$$y_D^I = \sqrt{P_S}h_{SD}x_S + n_D^I. \tag{4}$$

In this case, the received SNR at D required to successfully decode x_S is calculated as:

$$\gamma_D^I = \frac{|h_{SD}|^2 P_S}{N_0} = \Psi\gamma_{SD} \tag{5}$$

where $\Psi = \frac{P_S}{N_0}$ is the average transmit power to noise ratio.
If $P_h \geq P_{th}$, then B (Backscatter device) has enough energy to backscatter the signal to D. The received signal at D is then described by:

$$y_D^{II} = \sqrt{P_S}h_{SD}x_S + h_{BD}h_{SB}\sqrt{\beta P_S}x_B x_S + n_D^{II} \tag{6}$$

with $\mathbb{E}\{|x_B|^2\} = 1$.

The destination D first decodes the signal x_S by treating the backscattered signal as interference, with the received SINR (Signal-to-Interference-plus-Noise Ratio) given by:

$$\gamma_S = \frac{|h_{SD}|^2 P_S}{\beta P_S|h_{BD}|^2|h_{SB}|^2 + N_0} = \frac{|h_{SD}|^2\Psi}{\beta\Psi|h_{BD}|^2|h_{SB}|^2 + 1} \approx \frac{|h_{SD}|^2}{\beta|h_{BD}|^2|h_{SB}|^2} = \frac{\gamma_{SD}}{\beta\gamma_{SB}\gamma_{BD}} \tag{7}$$

Next, leveraging the SIC technique, x_S is subtracted from the composite received signal, i.e., $y_D^{III} = y_D^{II} - \sqrt{P_S}h_{SD}x_S + n_D^{III}$, here n_D^{III} denotes the AWGN introduced during the SIC operation, D can then decode the backscatter message x_B from B . Hence, the SNR of decoding x_B at D can be expressed as:

$$\gamma_B = \beta\Psi|h_{SB}|^2|h_{BD}|^2 = \beta\Psi\gamma_{SB}\gamma_{BD} \tag{8}$$

Finally, the backscatter signal can be successfully decoded when x_S and x_B are perfectly decoded at D. Thus, based on Equations (7) and (8), the end-to-end received SINR and SNR at D can be claimed by:

$$\gamma_D^{II} = \min(\gamma_S, \gamma_B) = \min\left(\frac{\gamma_{SD}}{\beta\gamma_{SB}\gamma_{BD}}, \beta\Psi\gamma_{SB}\gamma_{BD}\right) \tag{9}$$

3. PERFORMANCE ANALYSIS

3.1 Outage Probability Analysis

In this section, we provide a detailed and formal definition of the OP to evaluate the communication reliability of the proposed symbiotic radio system. An outage event occurs when the destination D is unable to successfully decode the intended information. Given the hardware constraints of the energy-constrained backscatter device B, the system performance is analyzed based on two mutually exclusive states of EH.

The first state represents a scenario where the backscatter device fails to harvest sufficient energy to activate its circuits ($P_h < P_{th}$). In this case, the system can only utilize the direct link from the source S. The second state occurs when B harvests enough energy ($P_h \geq P_{th}$), allowing it to function as a passive relay. In this symbiotic mode, D leverages the SIC technique to decode both primary and backscatter signals.

Formally, the OP of the proposed system is defined as the sum of the probabilities of these two independent events:

$$\text{OP} = \Pr\left(P_h < P_{th}, \gamma_D^I < \gamma_{th}\right) + \Pr\left(P_h \geq P_{th}, \gamma_D^{II} < \gamma_{th}\right) \tag{10}$$

where $\gamma_{\text{th}} = 2^{\text{R}} - 1$ is the threshold of the system and R is the target rate of the source. By employing the concept of normalized bandwidth ($\text{B} = 1$ Hz), the target transmission rate R is defined as the spectral efficiency in bits/s/Hz. According to the Shannon-Hartley theorem, the minimum SINR required to support this rate, defined as the system threshold γ_{th}, is obtained by solving $R = \log_2(1 + \gamma_{\text{th}})$, which yields the relation $\gamma_{\text{th}} = 2^{\text{R}} - 1$. This formulation provides a formal physical insight into the system's operation, where the overall reliability is modeled as a weighted sum of two independent energy states. It reveals that the system performance is fundamentally constrained by a critical coupling between the hardware-level energy-harvesting threshold P_{th} and the information theoretic-decoding requirement γ_{th}, characterizing the operational limits of battery-free backscatter-assisted relaying. By substituting the expressions for $\gamma_{\text{D}}^{\text{I}}$ (from Equation 5) and $\gamma_{\text{D}}^{\text{II}}$ (from equation (9) into equation (10), we gather the final expression for the outage probability:

$$\text{OP} = \underbrace{\Pr\left\{\gamma_{\text{SB}} < \frac{P_{\text{th}}}{\Psi(1-\beta)}, \Psi\gamma_{\text{SD}} < \gamma_{\text{th}}\right\}}_{P_1} + \underbrace{\Pr\left\{\gamma_{\text{SB}} \geq \frac{P_{\text{th}}}{\Psi(1-\beta)}, \min\left(\frac{\gamma_{\text{SD}}}{\beta\gamma_{\text{SB}}\gamma_{\text{BD}}}, \beta\Psi\gamma_{\text{SB}}\gamma_{\text{BD}}\right) < \gamma_{\text{th}}\right\}}_{P_2} \quad (11)$$

where $\Phi = \frac{P_{\text{th}}}{N_0}$.

From (11), P_2 is calculated as:

$$P_2 = \begin{cases} \Pr\left(\min\left(\frac{\gamma_{\text{SD}}}{\beta x\gamma_{\text{BD}}}, \beta\Psi x\gamma_{\text{BD}}\right) < \gamma_{\text{th}}\right) & , x \geqslant \frac{\Phi}{(1-\beta)\Psi} \\ 0 & , x < \frac{\Phi}{(1-\beta)\Psi} \end{cases}$$

$$= \int_{\frac{\Phi}{(1-\beta)\Psi}}^{+\infty} \underbrace{\Pr\left(\min\left(\frac{\gamma_{\text{SD}}}{\beta x\gamma_{\text{BD}}}, \beta\Psi x\gamma_{\text{BD}}\right) < \gamma_{\text{th}}\right)}_{\Theta} f_{\gamma_{\text{SB}}}(x)dx \quad (12)$$

From (12), Θ can be calculated as:

$$\Theta = 1 - \Pr\left(\min\left(\frac{\gamma_{\text{SD}}}{\beta x\gamma_{\text{BD}}}, \beta\Psi x\gamma_{\text{BD}}\right) \geq \gamma_{\text{th}}\right) \overset{(a)}{=} 1 - \Pr\left(\frac{\gamma_{\text{SD}}}{\beta x\gamma_{\text{BD}}} \geq \gamma_{\text{th}}, \beta\Psi x\gamma_{\text{BD}} \geq \gamma_{\text{th}}\right)$$

$$= 1 - \Pr\left(\frac{\gamma_{\text{th}}}{\beta\Psi x} \leq \gamma_{\text{BD}} \leq \frac{\gamma_{\text{SD}}}{\beta x\gamma_{\text{th}}}\right) = 1 - \int_0^{+\infty} \left[F_{\gamma_{\text{BD}}}\left(\frac{y}{\beta x\gamma_{\text{th}}}\right) - F_{\gamma_{\text{BD}}}\left(\frac{\gamma_{\text{th}}}{\beta\Psi x}\right)\right] f_{\gamma_{\text{SD}}}(y)dy \quad (13)$$

where step (a) is obtained by applying the property of the minimum of two random variables; i.e., $\Pr(\min(A, B) \geq \gamma_{\text{th}}) = \Pr(A \geq \gamma_{\text{th}}, B \geq \gamma_{\text{th}})$. By substituting Eq. (1) into Eq. (13) and performing several algebraic manipulations, the closed-form expression for Θ can be obtained as follows:

$$\Theta = 1 - \int_0^{+\infty} \left[\exp\left(-\frac{\lambda_{\text{BD}}\gamma_{\text{th}}}{\beta\Psi x}\right) - \exp\left(-\frac{\lambda_{\text{BD}}y}{\beta x\gamma_{\text{th}}}\right)\right] f_{\gamma_{\text{SD}}}(y)dy$$

$$= 1 - \exp\left(-\frac{\lambda_{\text{BD}}\gamma_{\text{th}}}{\beta\Psi x}\right) + \lambda_{\text{SD}} \int_0^{+\infty} \exp\left(-\frac{\lambda_{\text{BD}}y}{\beta x\gamma_{\text{th}}} - \lambda_{\text{SD}}y\right) dy \quad (14)$$

$$= 1 - \exp\left(-\frac{\lambda_{\text{BD}}\gamma_{\text{th}}}{\beta\Psi x}\right) + \frac{\lambda_{\text{SD}}\beta x\gamma_{\text{th}}}{\lambda_{\text{BD}} + \lambda_{\text{SD}}\beta x\gamma_{\text{th}}}$$

Substituting Eq. (14) into Eq. (12), we have:

$$P_2 = \int_{\frac{\Phi}{(1-\beta)\Psi}}^{+\infty} \left(1 - \exp\left(-\frac{\lambda_{\text{BD}}\gamma_{\text{th}}}{\beta\Psi x}\right) + \frac{\lambda_{\text{SD}}\beta x\gamma_{\text{th}}}{\lambda_{\text{BD}} + \lambda_{\text{SD}}\beta x\gamma_{\text{th}}}\right) \lambda_{\text{SB}}\exp(-\lambda_{\text{SB}}x)dx$$

$$= \exp\left(-\frac{\lambda_{\text{SB}}\Phi}{(1-\beta)\Psi}\right) + \lambda_{\text{SB}} \int_{\frac{\Phi}{(1-\beta)\Psi}}^{+\infty} \left(\frac{\beta x\gamma_{\text{th}}\lambda_{\text{SD}}}{\lambda_{\text{BD}} + \beta x\gamma_{\text{th}}\lambda_{\text{SD}}} - \exp\left(-\frac{\lambda_{\text{BD}}\gamma_{\text{th}}}{\beta\Psi x}\right)\right) \exp(-\lambda_{SB}x)dx. \quad (15)$$

However, the integral in Equation (15) is a tough task to find a closed-form expression. Hence, by applying the Gaussian-Chebyshev quadrature in [38], SOP can be approximated. As a result, with

$\phi_n = \cos\left(\frac{2n-1}{2N}\pi\right)$, P_2 can be reformulated as:

$$P_2 \approx \exp\left(-\frac{\lambda_{\mathrm{SB}}\Phi}{(1-\beta)\Psi}\right) + \frac{\lambda_{\mathrm{SB}}\pi^2}{4N}\sum_{n=1}^{N}\sqrt{1-\varphi_n^2}F\left(\tan\left((\varphi_n+1)\frac{\pi}{4}\right)+\frac{\Phi}{(1-\beta)\Psi}\right)\sec^2\left((\varphi_n+1)\frac{\pi}{4}\right)$$

$$= \exp\left(-\frac{\lambda_{\mathrm{SB}}\Phi}{(1-\beta)\Psi}\right) + \frac{\lambda_{\mathrm{SB}}\pi^2}{4N}\sum_{n=1}^{N}\left(\begin{array}{c}\sqrt{1-\varphi_n^2}\left(\begin{array}{c}\frac{\beta\left(\tan\left((\varphi_n+1)\frac{\pi}{4}\right)+\frac{\Phi}{(1-\beta)\Psi}\right)\gamma_{\mathrm{th}}\lambda_{\mathrm{SD}}}{\lambda_{\mathrm{BD}}+\beta\left(\tan\left((\varphi_n+1)\frac{\pi}{4}\right)+\frac{\Phi}{(1-\beta)\Psi}\right)\gamma_{\mathrm{th}}\lambda_{\mathrm{SD}}}\\ -\exp\left(-\frac{\lambda_{\mathrm{BD}}\gamma_{\mathrm{th}}}{\beta\Psi\left(\tan\left((\varphi_n+1)\frac{\pi}{4}\right)+\frac{\Phi}{(1-\beta)\Psi}\right)}\right)\end{array}\right)\\ \times\exp\left(-\lambda_{\mathrm{SB}}\left(\tan\left((\varphi_n+1)\frac{\pi}{4}\right)+\frac{\Phi}{(1-\beta)\Psi}\right)\right)\sec^2\left((\varphi_n+1)\frac{\pi}{4}\right)\end{array}\right) \quad (16)$$

Substituting Eq. (1) into Eq. (11) yields the calculation of P_1 as follows:

$$P_1 = \Pr\left(\gamma_{\mathrm{SB}} < \frac{\Phi}{(1-\beta)\Psi}, \gamma_{\mathrm{SD}} < \frac{\gamma_{\mathrm{th}}}{\Psi}\right) = \left(1-\exp\left(-\frac{\lambda_{\mathrm{SB}}\Phi}{(1-\beta)\Psi}\right)\right)\left(1-\exp\left(-\frac{\lambda_{\mathrm{SD}}\gamma_{\mathrm{th}}}{\Psi}\right)\right) \quad (17)$$

Substituting Eq. (16) and Eq. (17) into Eq. (11), we have:

$$\mathrm{OP} = \left(1-\exp\left(-\frac{\lambda_{\mathrm{SB}}\Phi}{(1-\beta)\Psi}\right)\right)\left(1-\exp\left(-\frac{\lambda_{\mathrm{SD}}\gamma_{\mathrm{th}}}{\Psi}\right)\right) + \exp\left(-\frac{\lambda_{\mathrm{SB}}\Phi}{(1-\beta)\Psi}\right)$$

$$+\frac{\lambda_{\mathrm{SB}}\pi^2}{4N}\sum_{n=1}^{N}\left(\begin{array}{c}\sqrt{1-\varphi_n^2}\left(\begin{array}{c}\frac{\beta\left(\tan\left((\varphi_n+1)\frac{\pi}{4}\right)+\frac{\Phi}{(1-\beta)\Psi}\right)\gamma_{\mathrm{th}}\lambda_{\mathrm{SD}}}{\lambda_{\mathrm{BD}}+\beta\left(\tan\left((\varphi_n+1)\frac{\pi}{4}\right)+\frac{\Phi}{(1-\beta)\Psi}\right)\gamma_{\mathrm{th}}\lambda_{\mathrm{SD}}}\\ -\exp\left(-\frac{\lambda_{\mathrm{BD}}\gamma_{\mathrm{th}}}{\beta\Psi\left(\tan\left((\varphi_n+1)\frac{\pi}{4}\right)+\frac{\Phi}{(1-\beta)\Psi}\right)}\right)\end{array}\right)\\ \times\exp\left(-\lambda_{\mathrm{SB}}\left(\tan\left((\varphi_n+1)\frac{\pi}{4}\right)+\frac{\Phi}{(1-\beta)\Psi}\right)\right)\sec^2\left((\varphi_n+1)\frac{\pi}{4}\right)\end{array}\right) \quad (18)$$

The closed-form expression in Equation (18) reveals several key mathematical insights into the system's behavior. First, the power-splitting factor β acts as a "mathematical pivot" that governs the trade-off between the activation probability of the backscatter device, which depends on $(1-\beta)$ and the energy threshold Φ, and the resulting signal quality at the destination, which is proportional to β. Second, the analytical structure highlights a "product-of-exponentials" characteristic arising from the cascaded channel gain $|h_{\mathrm{SB}}|^2|h_{\mathrm{BD}}|^2$. This indicates that a deep fade in either the forward link (S → B) or the backscatter link (B → D) will significantly dominate the overall outage performance. Finally, as the transmit SNR (Ψ) increases, the OP does not vanish to zero, but instead converges to a fixed performance floor. This demonstrates that the reliability of battery-free IoT devices is fundamentally constrained by the tight coupling between energy harvesting requirements (Φ) and the actual channel conditions.

4. NUMERICAL RESULTS AND SIMULATIONS

In this section, we provide numerical results to not only verify the accuracy of the proposed mathematical frameworks, but also discuss the behaviors of the considered systems under the impact of various important parameters by using the Monte-Carlo approach. To ensure the validity and practical relevance of our analysis, we used the simulation parameters such as those in [56]-[60]. These parameters are summarized in Table 2.

Figure 2 illustrates the OP *versus* the average transmit Signal-to-Noise Ratio (Ψ) in dB, considering

various required data rates ($R = \{0.15, 0.25, 0.5\}$bps/Hz). The close agreement between the theoretical analysis curves and the Monte-Carlo simulation results validates the accuracy of the closed-form outage probability expressions derived in the mathematical-analysis section. First, a monotonic decreasing trend in OP is observed as Ψ increases from 0 dB to 30 dB across all scenarios. This can be attributed to the fact that an increase in Ψ corresponds to higher transmit power P_S, which enables B to harvest sufficient energy to overcome the circuit-activation threshold (P_{th}). Simultaneously, the powers of both the reflected and direct signals at D are enhanced, thereby improving the received SINR and reducing the system-outage probability. Second, the required data rate R has a significant negative impact on the system performance. Specifically, at a fixed transmit power level (e.g., $\Psi = 10$ dB), as R increases from 0.15bps/Hz to 0.5bps/Hz, the OP rises sharply (indicated by the blue curve lying significantly higher than the red curve). This is because the SNR decoding threshold, defined as $\gamma_{\text{th}} = 2^R - 1$, increases with R. A higher γ_{th} necessitates superior channel conditions and sufficient harvested energy for successful decoding, consequently leading to a higher probability of outage events.

Table 2. Simulation parameters.

Symbol	Parameter name	Value
Ψ	Transmit power to noise ratio at S	0 to 30(dB)
Φ	Threshold of the transmit power to noise ratio at B	-10 to 5(dB)
R	Target rate	0.15 to 0.5bps/Hz
λ_{SB}	Mean of $\lvert h_{\text{SB}}\rvert^2$	0.25 to 4
λ_{BD}	Mean of $\lvert h_{\text{BD}}\rvert^2$	0.25 to 4
λ_{SD}	Mean of $\lvert h_{\text{SD}}\rvert^2$	0.25 to 2
N	The Gauss Chevbyshev parameter	80
β	The power-splitting factor	0 to 1

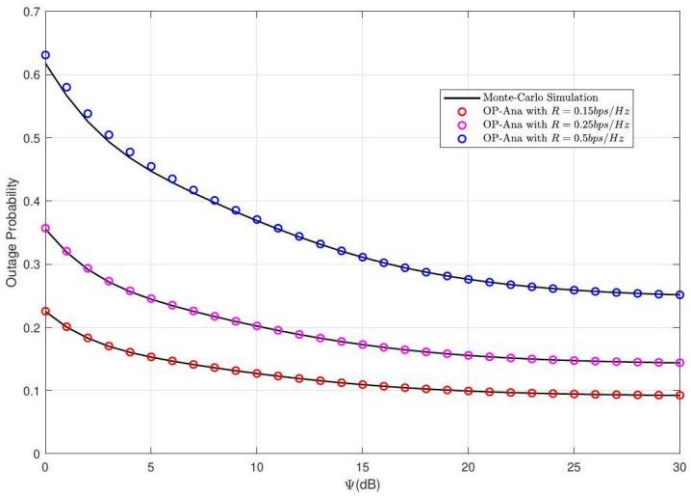

Figure 2. OP *versus* Ψ(dB), with varying R .

Figure 3 provides a detailed insight into how system characteristics affect the OP, with the distinction between linear and nonlinear models being prominently displayed. The adopted nonlinear energy-harvesting model is given below [61]-[62]

$$P_{\text{nEH}} = \frac{P_{\text{B}}^{\max}\left(1 - \exp(-\epsilon_1 P_{\text{h}} + \epsilon_1 \epsilon_0)\right)}{1 + \exp(-\epsilon_1 P_{\text{h}} + \epsilon_1 \epsilon_2)}, \tag{19}$$

where ϵ_0 represents the sensitivity threshold, ϵ_1 is the resistance parameter, and ϵ_2 denotes the capacitance parameter of the harvesting circuit; $P_{\text{B}}^{\max}$ is the maximum output supported by the circuit. Specifically, curves employing linear models consistently achieve superior performance, maintaining a significantly lower OP than their nonlinear counterparts, which suffer from signal distortion and component saturation. Similarly, imperfect SIC circumstances result in a larger OP because of residual interference from partially canceled signals. However, in these real-world situations, raising the average transmit power to noise ratio, Ψ, is a useful tactic to improve the OP and boost overall system performance in the low-power regime. The graph, however, also draws attention to a critical physical limit: this power enhancement is only effective up to a certain threshold; as Ψ increases, the OP

eventually enters an error floor brought on by dominant residual interference and nonlinearities, meaning that additional power increments no longer produce the notable OP reductions seen initially.

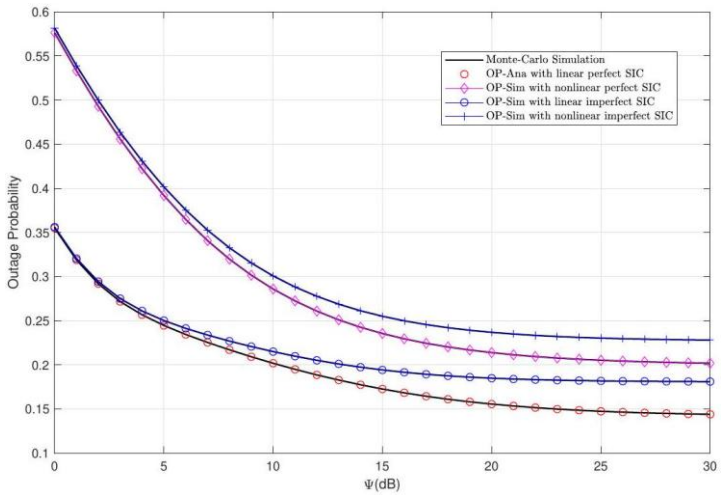

Figure 3. OP *versus* $\Psi(\mathrm{dB})$ for linear and nonlinear models under perfect and imperfect SIC scenarios.

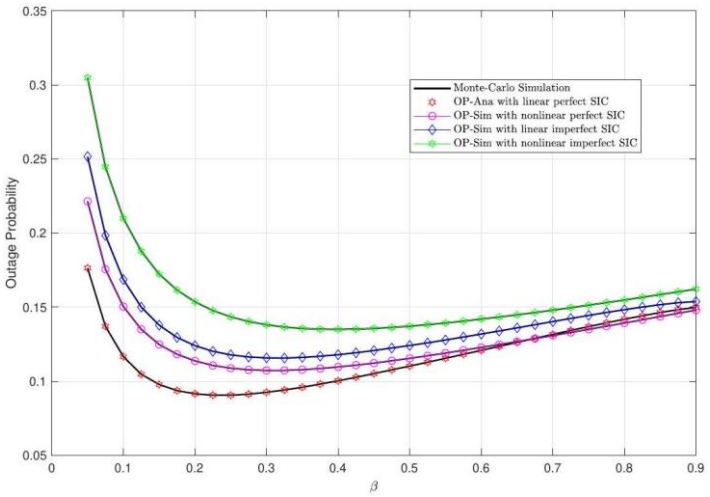

Figure 4. OP *versus* β for linear and nonlinear models under perfect and imperfect SIC scenarios.

Figure 4 illustrates the variation of the OP under the influence of the reflection coefficient β. The most prominent feature observed is the convex nature of the OP curves, which indicates the existence of a unique optimal value, denoted as β^*, that minimizes the system's outage probability. This behavior illustrates the fundamental trade-off between the EH process and the backscatter-communication efficiency. In the low β regime, a significant portion of the source power is allocated to EH, ensuring the activation of the backscatter device. However, the power fraction reserved for signal reflection is insufficient, resulting in a low SINR at the destination, thereby increasing the outage probability. Conversely, in the high β regime, while the reflected signal power is enhanced, the harvested energy at the backscatter device decreases. If the harvested power falls below the activation threshold ($P_h < P_{\mathrm{th}}$), the circuit fails to operate, leading to system outage. From the adopted non-linear model as shown in Equation (19), the optimal value $\beta_{\mathrm{h}}^* = \max\left(1 - \frac{\zeta}{\gamma_{SB}}, 0\right)$ is derived to ensure the successful transmission condition $P_{\mathrm{nEH}} \geq P_{\mathrm{th}}$. Furthermore, the comparison between different scenarios, such as imperfect SIC *versus* perfect SIC or linear *versus* non-linear models, yields results consistent with the previous findings in Figure 3. Specifically, the linear model and the perfect SIC scenario consistently establish an ideal performance limit with the lowest OP levels and *vice versa*.

Figure 5 illustrates the OP as a function of the channel parameters $\lambda_{\mathrm{SB}} = \lambda_{\mathrm{BD}}$ across different power-splitting factors (β). A notable observation is the non-monotonic behavior of the OP curves, which suggests that the system performance is governed by a trade-off inherent to the SIC decoding mechanism. Specifically, in the strong channel regime (low λ values), the backscattered signal acts as

significant interference to the direct link decoding; consequently, a smaller splitting factor (e.g., $= 0.15$) is preferable to mitigate this interference and lower the outage probability. Conversely, in the weak channel regime (high λ values), the system becomes power-limited, where the attenuation of the backscatter link compromises decodability. In this scenario, a larger splitting factor (e.g.,$= 0.5$) is required to boost the reflected-signal strength. The intersection of these performance curves demonstrates that there is no single optimal β for all channel conditions, highlighting the necessity for channel-adaptive power-splitting strategies to minimize system outage.

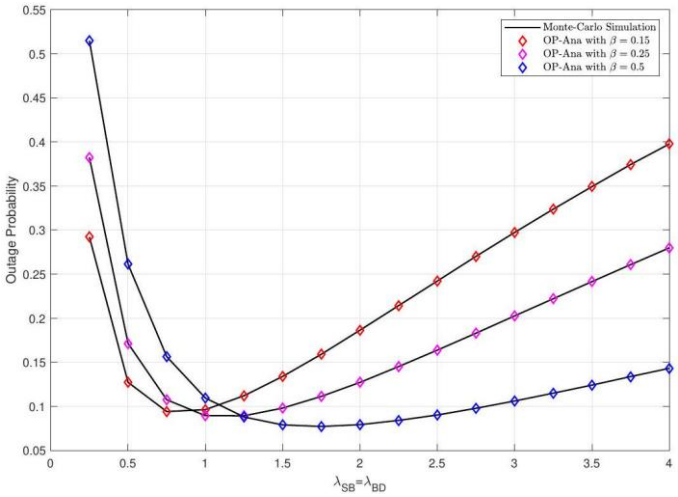

Figure 5. OP *versus* $\lambda_{\mathrm{SB}}, \lambda_{\mathrm{BD}}$, with varying β.

Figure 6 illustrates the OP as a function of the mean value of the random variable $\lambda(\lambda_{\mathrm{SB}} = \lambda_{\mathrm{BD}})$, representing the reciprocal of the mean channel gains for Rayleigh fading links. Given that the average power gain is defined as $\mathbb{E}[|\mathrm{h}|^2] = 1/\lambda$, values of $\lambda < 1$ signify favorable channel conditions with high average gains, whereas $\lambda > 1$ represents weak channel regimes or severe path loss scenarios. The graph reveals a critical performance trade-off: in the $\lambda < 1$ region, the OP is initially high, but drops rapidly as λ approaches 1, as the system moves away from being interference-limited, which typically hinders the SIC process. Conversely, as λ increases beyond the optimal point (around ≈ 1.5), the system becomes power-limited. These results are entirely consistent with the findings observed in Figure 3 and Figure 4, where the non-linear model, characterized by hardware parameters $\epsilon_0, \epsilon_1, \epsilon_2$ and the saturation power $P_{\mathrm{B}}^{\max}$, consistently yields a higher OP compared to the ideal linear model.

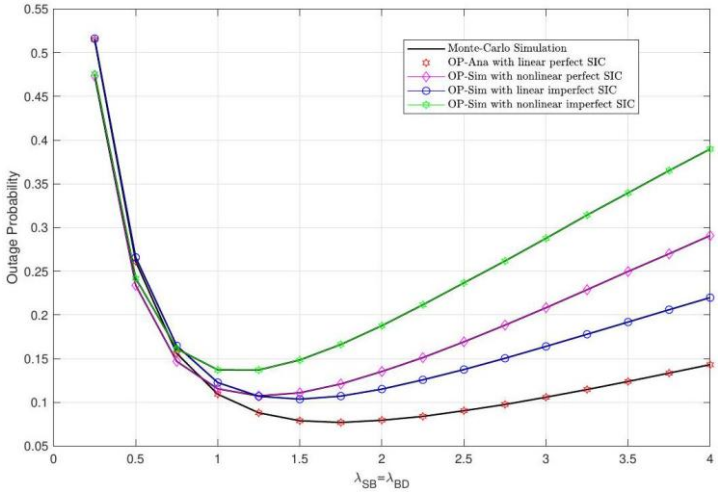

Figure 6. OP *versus* $\lambda_{\mathrm{SB}} = \lambda_{\mathrm{BD}}$ for linear and nonlinear models under perfect and imperfect SIC scenarios.

Figure 7 investigates the influence of the direct-link quality, denoted by λ_{SD}, on the system's OP under varying backscatter channel conditions ($\lambda_{\mathrm{SB}}, \lambda_{\mathrm{BD}}$). A general trend observed is the linear degradation of system performance (increasing OP) as λ_{SD} increases, corresponding to severe attenuation in the

direct link from the source to the destination. However, a counter-intuitive phenomenon is evident in the relative performance of the scenarios: the configuration with the strongest backscatter channels ($\lambda_{SB} = \lambda_{BD} = 0.5$, red curve) yields the highest outage probability, whereas the weaker backscatter channel configuration ($\lambda_{SB} = \lambda_{BD} = 1.5$, blue curve) results in the best performance. This observation substantiates the interference-limited nature of the SIC process; specifically, when the direct link is weak, a strong reflected signal from the backscatter device acts as severe interference, drastically reducing the SINR required to decode the source signal x_S. Consequently, in scenarios with poor direct-link connectivity, mitigating interference from the backscatter branch takes precedence over maximizing reflected power, thereby significantly enhancing the overall system reliability.

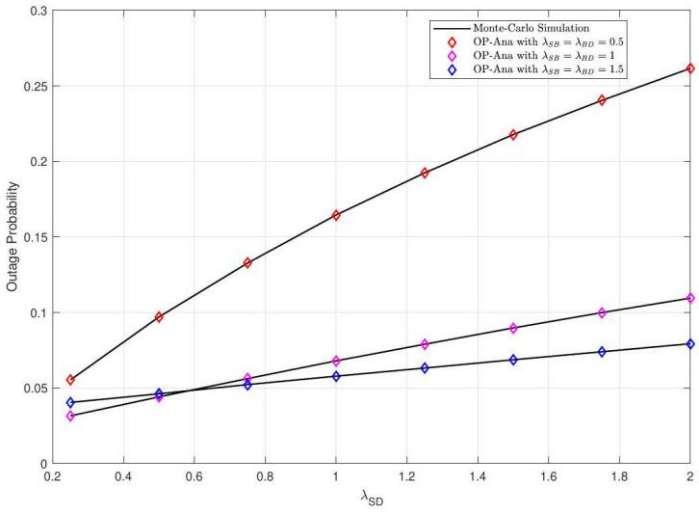

Figure 7. OP *versus* λ_{SD}, with varying $\lambda_{SB}, \lambda_{BD}$.

The OP as a function of the parameter λ_{SD}, which is the reciprocal of the mean channel gain for the direct source-to-destination link, is shown in Figure 8. In perfect-SIC scenarios, the OP increases steadily as λ_{SD} rises from 0.25 to 2, indicating that overall system performance decreases as the direct-channel quality deteriorates due to the weakened reliability of the direct-transmission path. The results show different system behaviors depending on interference-cancellation proficiency. Conversely, imperfect SIC scenarios exhibit an optimal point (minimum OP) around $\lambda_{SD} \approx 0.75$ to 1.0. In the low λ_{SD} regime, despite high channel gains, the OP rises, because the system becomes interference-limited, exceeding the capabilities of imperfect interference cancellation; meanwhile, beyond the optimal threshold, the OP increases again as the system enters the power-limited regime. Consistent with Figures 3, 4, and 6, the non-linear model consistently exhibits higher OP than the ideal linear model due to physical constraints, such as power saturation P_B^{max} and activation thresholds of the energy-harvesting circuit.

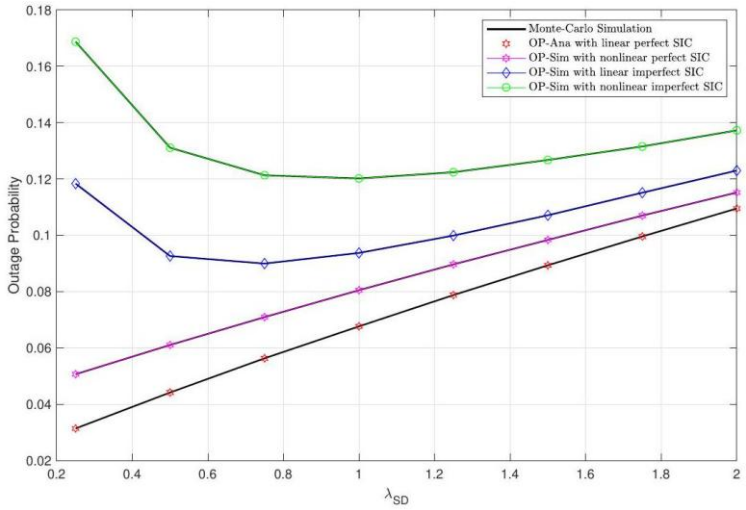

Figure 8. OP *versus* λ_{SD} for linear and nonlinear models under perfect and imperfect-SIC scenarios.

Figure 9 illustrates the variation of the OP as a function of the parameter Ψ (in dB), representing the transmit power or SNR of the system. The results show that as Ψ increases from 0 to 30 dB , the outage probability for all scenarios decreases significantly, demonstrating that increasing the transmit power is a direct solution for enhancing the reliability of the transmission link, which is consistent with the findings in Figures 2 and 3. Furthermore, the linear model consistently achieves a much lower OP compared to the corresponding nonlinear model due to physical limits imposed by hardware parameters $\epsilon_0, \epsilon_1, \epsilon_2$, similar to previous findings. Notably, emphasizing the impact of CSI, the gap between perfect-CSI and imperfect-CSI scenarios indicates that the system is highly sensitive to the accuracy of channel estimation. In practice, it is difficult to obtain perfect CSI due to channel-estimation errors (CEEs); therefore, we adopt the linear minimum mean square error method as suggested in [63] to obtain the CSI. Consequently, the communication channels are modeled following the framework in [64] as: $\hat{h}_i = h_i + e_i$ where $i \in \{\text{SD}, \text{BD}, \text{SB}\}$ denotes the communication links, $\hat{h}_i$ is the estimated channel, and $e_i \sim CN(0, \mu_i)$ represents the CEE with error variance μ_i. As Ψ approaches 30 dB, an error floor begins to emerge, where further power increments no longer yield significant reductions in OP due to the dominance of residual interference, channel-estimation inaccuracies, and nonlinear components.

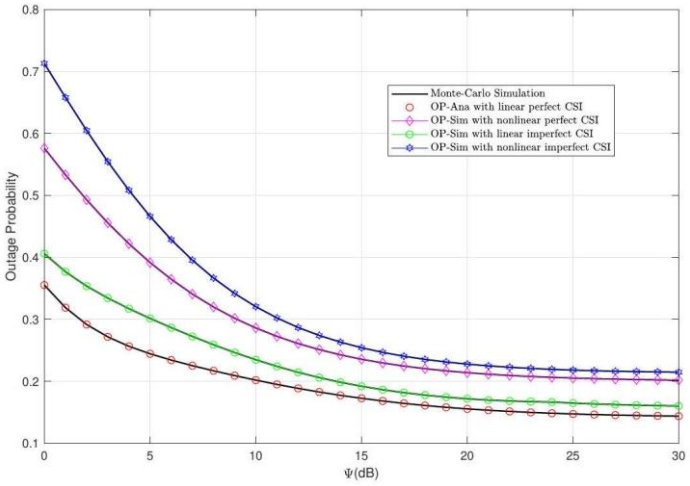

Figure 9. OP *versus* Ψ(dB) for linear and nonlinear models under perfect and imperfect-CSI scenarios.

Table 3 summarizes the key system parameters and their impacts on the OP, highlighting the underlying physical insights revealed by the analytical and numerical results. This table provides an intuitive overview of how transmit power, target rate, power splitting, channel conditions, energy-harvesting modeling, and SIC/CSI quality jointly influence system performance.

Table 3. Summary of key insights and parameter impacts on system performance.

Parameter	**Trend**	**Key Physical Insight**
Transmit SNR (Ψ)	↘ OP	Higher power facilitates energy harvesting and improves SINR, but leads to an error floor at high values due to residual interference (Figs. 2, 3, 9).
Target Rate (R)	↗ OP	Increasing R raises the decoding threshold $\gamma_{\text{th}} = 2^{\text{R}} - 1$, requiring higher channel quality for success (Fig. 2).
Splitting Factor (β)	Convex	Represents the trade-off between energy harvesting (for activation) and reflection (for signal quality) (Figs. 4).
Channel Gains (λ)	Non-monotonic	System is interference-limited in strong channels ($\lambda < 1$) and power-limited in weak channels ($\lambda > 1.5$) (Figs. 5, 7, 6, 8).
EH Modeling	Value: OP of (linear < non-linear)	Linear model acts as an ideal upper bound, while non-linear hardware (saturation/thresholds) degrades performance (Figs. 3, 4, 6, 8, 9).
SIC/CSI Quality	Value: OP of (perfect < imperfect)	Residual interference and estimation errors significantly increase the outage probability in realistic scenarios (Figs. 3, 4, 6, 8, 9).

5. CONCLUSIONS

This paper has presented a comprehensive performance analysis of an ambient backscatter-assisted passive relaying system. We successfully derived accurate closed-form expressions for the OP over Rayleigh fading channels and validated the theoretical framework through extensive Monte-Carlo simulations. The study rigorously examined the influence of general system parameters, the most significant findings reveal how the interplay between non-linear energy harvesting and imperfect SIC/CSI dictates the system's reliability limits. Specifically, the results demonstrated a clear convex relationship between the OP and the power-splitting factor, confirming the existence of a unique optimal value that balances energy harvesting and signal reflection. Furthermore, our analysis underlines the detrimental impact of residual interference, which leads to the emergence of inevitable error floors in the high-SNR regime. A non-monotonic performance trend was also observed regarding the backscatter-link quality, revealing an optimal operating regime where the system effectively balances signal strength against the interference floor. These insights provide a robust quantitative tool for the design of ultra-energy-efficient IoT networks. For future work, we aim to extend this analytical framework to more complex multi-node scenarios and explore advanced beamforming techniques to further mitigate the identified performance bottlenecks.

REFERENCES

[1] S. Dang, O. Amin, B. Shihada and M.-S. Alouini, "What Should 6G Be?," Nature Electronics, vol. 3, no. 1, pp. 20-29, DOI: 10.1038/s41928-019-0355-6, Jan. 2020.

[2] H. Pennanen et al., "6G: The Intelligent Network of Everything," IEEE Access, vol. 13, pp. 1319-1421, DOI: 10.1109/ACCESS.2024.3521579, 2025.

[3] W. Jiang, B. Han, M. A. Habibi and H. D. Schotten, "The Road towards 6G: A Comprehensive Survey," IEEE Open Journal of the Communications Society, vol. 2, pp. 334-366, 2021.

[4] W. Wu et al., "A Survey on Ambient Backscatter Communications: Principles, Systems, Applications and Challenges," Computer Networks, vol. 216, p. 109235, DOI: 10.1016/j.comnet.2022.109235, 2022.

[5] M. A. Jamshed et al., "Artificial Intelligence, Ambient Backscatter Communication and Non-terrestrial Networks: A 6G Commixture," IEEE Internet of Things Magazine, vol. 8, no. 2, pp. 88-94, 2025.

[6] C. Liaskos et al., "Realizing Ambient Backscatter Communications with Intelligent Surfaces in 6G Wireless Systems," IEEE Wireless Communications, vol. 29, no. 1, pp. 178-185, Feb. 2022.

[7] H.-N. Nguyen et al., "Secure Performance Analysis of Satellite-terrestrial Networks-assisted Backscatter Device," Jordanian J. of Computers and Inform. Techn. (JJCIT), vol. 11, no. 4, pp. 484-498, Dec. 2025.

[8] D. L. Galappaththige, F. Rezaei, C. Tellambura and S. Herath, "RIS-empowered Ambient Backscatter Communication Systems," IEEE Wireless Communications Letters, vol. 12, no. 1, pp. 173-177, 2023.

[9] H. Yang et al., "A RIS-segmented Symbiotic Ambient Backscatter Communication System," IEEE Transactions on Vehicular Technology, vol. 73, no. 1, pp. 812-825, 2024.

[10] A.-T. Le et al., "Performance Analysis of RIS-assisted Ambient Backscatter Communication Systems," IEEE Wireless Communications Letters, vol. 13, no. 3, pp. 791-795, 2024.

[11] S. Jia et al., "Secrecy Performance Analysis of UAV-assisted Ambient Backscatter Communications with Jamming," IEEE Transactions on Wireless Communications, vol. 23, no. 12, pp. 18111-18125, 2024.

[12] J. Liu et al., "Intelligent Reflecting Surface-aided Covert Ambient Backscatter Communication," IEEE Trans. on Communications, vol. 72, no. 6, pp. 3558-3571, 2024.

[13] T. N. Nguyen et al., "On the Performance of Secured Ambient Backscatter Communications to Protect Digital Content and Copyrights," IEEE Access, vol. 13, pp. 195385-195400, 2025.

[14] H. Zhu et al., "Machine Learning-based Blind Signal Detection for Ambient Backscatter Communication Systems," IEEE Trans. on Cognitive Comm. and Netw., vol. 11, no. 2, pp. 1172-1183, 2025.

[15] J. Chen, Q. Guan, Y. Rong and H. Yu, "Detections for Ambient Backscatter Communications Systems with Dynamic Sources," IEEE Transactions on Communications, vol. 73, no. 9, pp. 7941-7951, 2025.

[16] J. Liao, T. Zhang, K. Ruttik, R. Jäntti and D.-T. Phan-Huy, "Ambient Backscatter Communication in LTE Uplink Sounding Reference Signal," arXiv preprint, DOI: 10.48550/arXiv.2501.10952, 2025.

[17] M. Tran et al., "Outage Analysis of a Hybrid Relay-Backscatter Communication System with Energy Harvesting for IoT and 6G Networks," IEEE Access, vol. 13, pp. 188605-188617, 2025.

[18] X. Liu, H. Wang, K. Zheng and K. Chi, "Throughput Maximization of IoT Transmission in STAR-RIS-aided Symbiotic Radio Networks," IEEE Internet of Things J., vol. 13, no. 2, pp. 3371-3388, Jan. 2026.

[19] L. S. Phu et al., "Enhancing Short-packet Communications: BLER Performance in RIS-assisted Ambient Backscatter NOMA Systems," PLOS ONE, vol. 20, no. 8, pp. 1-26, 2025.

[20] Y. Ye, L. Shi, X. Chu, G. Lu and S. Sun, "Mutualistic Cooperative Ambient Backscatter Communications under Hardware Impairments," IEEE Trans. on Communications, vol. 70, no. 11, pp. 7656-7668, 2022.

[21] K. Zheng et al., "DDPG-based Joint Time and Energy Management in Ambient Backscatter-assisted

Hybrid Underlay CRNs," IEEE Trans. on Communications, vol. 71, no. 1, pp. 441-456, Jan. 2023.

[22] T.-H. T. Pham et al., "Performance Analysis in D2D Partial NOMA-assisted Backscatter Communication," Advances in Electrical and Electronic Engineering, vol. 23, no. 3, pp. 250-262, 2025.

[23] Q.-S. Nguyen et al., "Power Beacon-assisted Energy Harvesting in D2D Network under Co-channel Interferences: Symbol Error Rate Analysis," Jordanian Journal of Computers and Information Technology (JJCIT), vol. 11, no. 4, pp. 517-532, 2025.

[24] X. Liu, J. Xu, K. Zheng, G. Zhang, J. Liu and N. Shiratori, "Throughput Maximization with an AoI Constraint in Energy Harvesting D2D-enabled Cellular Networks: An MSRA-TD3 Approach," IEEE Trans. on Wireless Communications, vol. 24, no. 2, pp. 1448-1466, Feb. 2025.

[25] G. Moloudian et al., "RF Energy Harvesting Techniques for Battery-less Wireless Sensing, Industry 4.0, and Internet of Things: A Review," IEEE Sensors Journal, vol. 24, no. 5, pp. 5732-5745, 2024.

[26] B. Y. León Ávila et al., "Energy Harvesting Techniques for Wireless Sensor Networks: A Systematic Literature Review," Energy Strategy Reviews, vol. 57, p. 101617, 2025.

[27] J. Zhou et al., "Metamaterials and Metasurfaces for Wireless Power Transfer and Energy Harvesting," Proceedings of the IEEE, vol. 110, no. 1, pp. 31-55, DOI: 10.1109/JPROC.2021.3127493, 2022.

[28] Y. Albaihani et al., "Optimal Antenna Design for Wireless Energy Harvesting System in ISM Band," Results in Physics, vol. 73, p. 108255, DOI: 10.1016/j.rinp.2025.108255, 2025.

[29] P. Zhang, X. Zhang and L. Li, "An Optically Transparent Metantenna for RF Wireless Energy Harvesting," IEEE Transactions on Antennas and Propagation, vol. 70, no. 4, pp. 2550-2560, 2022.

[30] Q.-S. Nguyen, C.-H. Tran, T.-D. Tran, M. Tran and B.-S. Kim, "Securing Wireless Communications with Energy Harvesting and Multi-antenna Diversity," Jordanian Journal of Computers and Information Technology (JJCIT), vol. 11, no. 2, pp. 197-210, DOI: 10.5455/jjcit.71-1732244909, Jun. 2025.

[31] B. V. Minh et al., "Self-energy Recycling in DF Full-duplex Relay Network: Security-Reliability Analysis," Advances in Electrical and Electronic Engineering, vol. 22, no. 1, pp. 86-96, 2024.

[32] S. Ghosh et al., "On the Performance of End-to-end Cooperative NOMA-based IoT Networks with Wireless Energy Harvesting," IEEE Internet of Things Journal, vol. 10, no. 18, pp. 16253-16270, 2023.

[33] D. Bepari et al., "Uplink Performance Analysis of Wireless Energy Harvesting-enabled NOMA-based Networks," Mobile Networks and Applications, vol. 29, no. 3, pp. 856-866, 2024.

[34] T. N. Nguyen et al., "On the Dilemma of Reliability or Security in Unmanned Aerial Vehicle Communications Assisted by Energy Harvesting Relaying," IEEE J. on Selected Areas in Comm., vol. 42, no. 1, pp. 52-67, 2024.

[35] X. Liu et al., "AoI-minimal Clustering, Transmission and Trajectory Co-design for UAV-assisted WPCNs," IEEE Trans. on Vehicular Technology, vol. 74, no. 1, pp. 1035-1051, Jan. 2025.

[36] K. Ntontin et al., "Wireless Energy Harvesting for Autonomous Reconfigurable Intelligent Surfaces," IEEE Trans. on Green Communications and Networking, vol. 7, no. 1, pp. 114-129, 2023.

[37] M. Poposka et al., "Design Optimization of RF Energy Harvesting Networks for Federated Learning," Proc. 2024 Int. Balkan Conf. Commun. Networking (BalkanCom), pp. 58-62, DOI: 10.1109/BalkanCom61808.2024.10557202, 2024.

[38] B. V. Minh, N. H. K. Nhan, T.-H. T. Pham, M. Tran and S.-W. Kim, "Physical Layer Security in Wireless Sensors Networks with Friendly Jammer: Secrecy Outage Probability Analysis," Advances in Electrical and Electronic Engineering, vol. 22, no. 4, pp. 387-398, DOI: 10.15598/aeee.v22i4.5840, 2024.

[39] M. Malik, A. Kothari and R. Pandhare, "Smart Military Logistics Based on Internet of Things and Energy Harvesting," Advances in Electrical & Electronic Engineering, vol. 23, no. 2, 2025.

[40] R. Du et al., "Comparing Backscatter Communication and Energy Harvesting in Massive IoT Networks," IEEE Transactions on Wireless Communications, vol. 21, no. 1, pp. 429-443, 2022.

[41] J. Zan et al., "Stochastic Geometry Based Performance Study for Wireless Powered Backscatter Communications," IEEE Trans. on Vehicular Technology, vol. 71, no. 10, pp. 11136-11149, 2022.

[42] T. Jiang et al., "Backscatter Communication Meets Practical Battery-free Internet of Things: A Survey and Outlook," IEEE Communications Surveys & Tutorials, vol. 25, no. 3, pp. 2021-2051, 2023.

[43] H. Ma et al., "Reconfigurable Intelligent Surface with Energy Harvesting Assisted Cooperative Ambient Backscatter Communications," IEEE Wireless Comm. Letters, vol. 11, no. 6, pp. 1283-1287, 2022.

[44] X. Liu, X. Li, K. Zheng and J. Liu, "AoI Minimization of Ambient Backscatter-assisted EHCRN with Cooperative Spectrum Sensing," Computer Networks, vol. 245, p. 110389, 2024.

[45] K. Zheng et al., "A Hybrid Communication Scheme for Throughput Maximization in Backscatter-aided Energy Harvesting Cognitive Radio Networks," IEEE IoT J., vol. 10, no. 18, pp. 16194-16208, 2023.

[46] X. Liu etal., "Optimal Time Allocation for Backscatter-aided Relay Cooperative Transmission in Wireless-powered Heterogeneous CRNs," IEEE IoT J., vol. 10, no. 18, pp. 16209-16224, 2023.

[47] A. Iqbal and T.-J. Lee, "Opportunistic Backscatter Communication Protocol Underlying Energy Harvesting IoT Networks," IEEE Access, vol. 11, pp. 89568-89580, 2023.

[48] W.-J. Wang, K. Xu, Y. Yan and L. Chen, "Relay Selection-based Cooperative Backscatter Transmission with Energy Harvesting: Throughput Maximization," IEEE Wireless Communications Letters, vol. 11, no. 7, pp. 1533-1537, DOI: 10.1109/LWC.2022.3179019, 2022.

[49] X. Liu et al., "Throughput Maximization of Wireless-powered Communication Network with Mobile Access Points," IEEE Transactions on Wireless Communications, vol. 22, no. 7, pp. 4401-4415, 2023.
[50] B. Lyu, C. You, Z. Yang and G. Gui, "The Optimal Control Policy for RF-powered Backscatter Communication Networks," IEEE Trans. on Vehicular Technology, vol. 67, no. 3, pp. 2804-2808, 2018.
[51] P. Ghosh, H. Yenna, S. D. Roy and S. Kundu, "Outage Analysis of an EH Relay Aided Network with Ambient-Backscattering," Proc. IEEE Int. Conf. Electronics, Computing and Communication Technologies (CONECCT), pp. 1-6, DOI: 10.1109/CONECCT62155.2024.10677243, 2024.
[52] L. Shi, J. Shi, Y. Ye, G. Zheng and G. Lu, "Ambient Backscatter Communication with HARQ Assisted Hybrid Long-short Packets," IEEE Communications Letters, vol. 28, no. 10, pp. 2258-2262, 2024.
[53] J. Shi et al., "Performance Analysis for Ambient Backscatter Communications with Hybrid Long-short Packets," IEEE Wireless Communications Letters, vol. 13, no. 5, pp. 1325-1329, 2024.
[54] X. Song et al., "Relay Assisted Cooperative Ambient Backscatter Communication with Hybrid Long-short Packets," IEEE Trans. on Vehicular Technology, vol. 73, no. 9, pp. 12890-12903, 2024.
[55] P. Ghosh, S. D. Roy and S. Kundu, "Energy Harvesting-assisted Two-user Cooperative NOMA with Ambient Backscattering," Int. J. of Communication Systems, vol. 38, no. 4, p. e6133, 2025.
[56] B. C. Nguyen et al., "Improving the Performance of Spatial Modulation Fullduplex Relaying System with Hardware Impairment Using Transmit Antenna Selection," IEEE Access, vol. 8, pp. 20191-20202, 2020.
[57] M. H. Tran, B. C. Nguyen and T. T. Phuong, "Outage Analysis of RF Energy Harvesting Cooperative Communication Systems over Nakagami-fading Channels with Integer and Non-Integer m," IEEE Transactions on Vehicular Technology, vol. 69, no. 3, pp. 2785-2801, Jan. 2020.
[58] T. N. Nguyen, T. T. Phuong and M. Voznak, "Wireless Energy Harvesting Meets Receiver Diversity: A Successful Approach for Two-way Half-duplex Relay Networks over Block Rayleigh Fading Channel," Computer Networks, vol. 172, p. 107176, DOI: 10.1016/j.comnet.2020.107176, May 2020.
[59] H. Nguyen et al., "Security-Reliability Analysis in CR-NOMA IoT Network under I/Q Imbalance," IEEE Access, vol. 11, pp. 119045-119056, DOI: 10.1109/ACCESS.2023.3327789, Nov. 2023.
[60] N.-T. Nguyen et al., "Performance Analysis of NOMA-based Hybrid Satellite-Terrestrial Relay System Using mmWave Technology," IEEE Access, vol. 11, pp. 10696-10707, Jan. 2023.
[61] Y. Khan et al., "Secrecy Analysis of Energy Harvesting Backscatter Communication Networks with Multiple Eavesdroppers and Different Tag Selection Schemes," IEEE Transactions on Green Communications and Networking, pp. 1-15, DOI: 10.1109/TGCN.2025.3563107, 2025.
[62] T. T. Duy et al., "On the Performance of the Coverage Probability of LoRa Networks with Non-linear Energy Harvesting," Proc. 2024 Int. Conf. on Advanced Technologies for Communications (ATC), pp. 722-726, DOI: 10.1109/ATC63255.2024.10908157, Ho Chi Minh City, Vietnam, 2024.
[63] X. Li et al., "Security and Reliability Performance Analysis of Cooperative Multi-relay Systems with Nonlinear Energy Harvesters and Hardware Impairments," IEEE Access, vol. 7, pp. 102644-102661, DOI: 10.1109/ACCESS.2019.2930664, 2019.
[64] T. N. Nguyen et al., "Security and Reliability Analysis of Satellite-terrestrial Multi-relay Networks with Imperfect CSI," IEEE Systems Journal, vol. 17, no. 2, pp. 2824-2835, Aug. 2022.

ملخص البحث:

تتناول هذه الورقة بِنية مبتكرة تستخدم بروتوكولات حصاد الطّاقة لدمْج تقنية الاتّصال بالتّشتُّت الخلفي المحيط كجهاز ترحيلٍ سلبي. وهذا الجهاز ذو الطّاقة المحدودة يستخدم آليةً لتقسيم الطّاقة لتفعيل الدّارة. ويتمثل الاسهام لهذا العمل في تطوير صيغ رياضية مغلقة جديدة ودقيقة لاحتمالية انقطاع النّظام عبر قنوات (رايلي) المتلاشية. وأجريت محاكاة (مونتي كارلو) مكثّفة للتّحقّق بدقّةٍ من صحّة الإطار التّحليلي المقترح. وكشف التّحليل مُفاضلاتٍ مهمّة بين موثوقية الإرسال وكفاءة حصاد الطّاقة، الأمر الّذي يوفّر رؤى قيمّة لتحسين استخدام الموارد في شبكات إنترنت الأشياء منخفضة الطّاقة المستقبلية. وأظهرت النّتائج إمكانية التّخفيف الفعّال من الآثار السّلبية لعدم اكتمال إلغاء التّداخل المتتالي و/أو عدم اكتمال معلومات حالة القناة عن طريق زيادة طاقة الإرسال و/أو التّشغيل عند القيمة المثلى لمعامل الانعكاس. واتّضح أنّ فجوة الأداء بين نظامي (SIC) و(CSI) المثاليّيْن وغير المثاليّيْن صغيرة نسبياً. وأخيراً، نبرهن تحليلياً أنّ نموذج حصاد الطّاقة الخطّي يمثّل حدّاً أعلى لنموذج حصاد الطّاقة غير الخطّي العملي.